

Quantum heat engine in the optomechanical system with mechanical parametric drive

Zhen-Yang Peng^{1,2,*} and Ying-Dan Wang^{2,3,†}

¹*Wilczek Quantum Center, School of Physics and Astronomy,
Shanghai Jiao Tong University, 200240, China*

²*CAS Key Laboratory of Theoretical Physics, Institute of Theoretical Physics,
Chinese Academy of Sciences, Beijing 100190, China*

³*School of Physical Sciences, University of Chinese Academy of Sciences, Beijing 100049, China*

(Dated: December 17, 2024)

Abstract

We consider a quantum Otto-type heat engine constructed in an optomechanical system with which the cavity is chosen as the working substance. The cavity can effectively be coupled with hot thermal baths in nonequilibrium steady-states via optomechanical interaction. The mechanical mode with parametric drive fuels the cavity, and the utilization efficiency of energy is discussed. To obtain higher efficiency in finite time evolution, we use the shortcuts-to-adiabaticity method in work generation processes. The modified thermal efficiencies are obtained by numerical simulation. Such a system provides potential applications in quantum heat transfer and energy utilization in quantum devices.

I. INTRODUCTION

Quantum thermodynamics [9] is an extension of the standard thermodynamics that the physical objects with the inclusion of quantum effects and usually in non-equilibrium situations. This rapidly growing research area not only provides the fundamental viewpoint on the understanding of quantum systems but also has great potential for nano-scale applications. As one of the important topics, quantum heat engines (QHEs) are important devices that convert heat to mechanical work for quantum systems [6, 15, 33–35]. Because of the quantum effects of the working substance or the heat baths, QHEs have unusual properties. For the cyclic heat engines to generate mechanical output work in a thermodynamical cycle, the efficiency of QHEs will surpass the standard limit defined in the classical thermodynamics [10, 11, 15]. While for the steady-state heat engines that transfer energies from the hot baths to the cold baths, the QHE suggests some effects violated the classical laws of thermodynamics [13, 14], although it is correct in the quantum mechanical viewpoint.

For the fluctuation heat engines [18], the probability distribution of work output [7, 8] and heat absorbed [19] per thermodynamical cycle and the efficiency fluctuations [16, 17, 20, 21] have been studied theoretically and experimentally. Because of the quantum non-adiabatic qualities, these distributions have unconventional behaviors, at the same time, the average work output and efficiencies will be suppressed.

To design a quantum heat engine with non-zero power output, the finite-time thermodynamical processes will be taken into consideration for the optimization of the QHE. The finite-time QHE has been discussed for the finite-time adiabatic processes [24, 25], and by the technique of shortcut-to-adiabatically (STA) [5, 22, 23].

These two strategies lead to higher efficiencies and non-zero power.

In this paper, we have proposed a quantum harmonic heat engine constructed in an optomechanical system with an external mechanical parametric drive [3]. Unlike the other studies for QHEs in the optomechanical systems [26–29], the cavity is chosen as working substance. In particular, the mechanical mode has been considered as the quantum object that provides external energies, which is equivalent to the fuel as the component for classical machines. The heat flux for the total system in the cavity thermalization process is discussed, and the cyclic work extraction can be achieved from a single physical thermal reservoir coupled to the cavity. Due to the interaction of optomechanics, non-equilibrium behavior is induced, resulting in this counter-intuitive phenomena [12]. We then construct the Otto-type cycle for the heat engine by modulating the parametric driving strength [4]. Finally, the extra heat absorption induced by the optomechanical interaction in the work generation strokes has been considered, and the corresponding thermal efficiencies within and without the STA method, are analyzed.

This paper is organized as follows: in Sec. II we first introduced the model, then the heat flux between the working fluid photons and the fuelled phonons is analyzed, and the quantum Otto cycle in this model is constructed; In Sec. III the efficiencies for the different cases are discussed. Conclusions and discussions are given in Sec. IV. Some technical details are given in the Appendices.

II. MODEL AND THERMODYNAMIC CYCLE

We consider an optomechanical system with a parametric drive applied to mechanics [3, 4] and a coherent laser drive $H_{\text{dri}} = Aae^{i\omega_L t} + \text{h.c.}$, under the standard

* pengzhenyang@sjtu.edu.cn

† yingdan.wang@itp.ac.cn

linearization, the system has the effective Hamiltonian

$$H(t) = H_a + H_b + G(ab^\dagger + a^\dagger b) + \frac{i}{2}\lambda(b^{\dagger 2}e^{-i2\omega_M t} - b^2 e^{i2\omega_M t}), \quad (1)$$

where $H_a = \Delta(a^\dagger a + 1/2)$, $H_b = \omega_M(b^\dagger b + 1/2)$, Δ is the cavity detuning, ω_M is the intrinsic frequency for mechanical mode, G is the collective coupling, λ indicates the parametric drive strength. The cavity mode is chosen as the quantum harmonic heat engine, with the detuning changing as work producing. Here the cavity detuning $\Delta = \omega_c - \omega_L$ can be tuned *in situ*. The dynamics of the total optomechanical system can be described by the following master equation:

$$\dot{\rho} = -i[H(t), \rho] + \mathcal{L}_{\text{diss}}\rho, \quad (2)$$

$$\begin{aligned} \mathcal{L}_{\text{diss}}\rho = & \kappa(\bar{n}_c + 1)D[a]\rho + \kappa\bar{n}_c D[a^\dagger]\rho \\ & + \gamma(\bar{n} + 1)D[b]\rho + \gamma\bar{n}D[b^\dagger]\rho. \end{aligned} \quad (3)$$

Based on the second law of thermodynamics, a heat engine must be in contact with at least two thermal baths, with different thermal occupations \bar{n}_c and decay rate κ in corresponding thermodynamical processes. However, if an auxiliary term that interacts with the heat engine is considered, the interaction provides an additional excitation for the heat engine, which is equivalent to an effective hot (cold) reservoir only coupled with the heat engine. In our work, the optomechanical interaction and the mechanical parametric drive would excite the cavity into higher occupations at the non-equilibrium steady-states, and thus produce an effective hot thermal bath for the heat engine. Therefore, the mechanical mode with parametric drive here fuels the cavity, and the interaction term transports the energy from the *fuel* to the engine.

A. Heat flux within the parametric drive

As mentioned above, the mechanical mode acts as quantum fuel which provides effective hot reservoirs. Meanwhile, the cavity extracts heat from the mechanical mode via the optomechanical interaction. Naturally, the utilization efficiency of the energy of the quantum fuel, which can be defined as the ratio of heat flux transforming into the heat engine to the total heat flux injected into the mechanical mode, is one of the characteristics of quantum heat engines.

Based on the energy conservation, the heat flux for both the cavity and the mechanical mode has the form [2]

$$\frac{d\langle H_a \rangle}{dt} = \dot{Q}_{b \rightarrow a} + \dot{Q}_a^\uparrow + \dot{Q}_a^\downarrow, \quad (4a)$$

$$\frac{d\langle H_b \rangle}{dt} = \dot{Q}_{a \rightarrow b} + \dot{Q}_{\text{PD}} + \dot{Q}_b^\uparrow + \dot{Q}_b^\downarrow. \quad (4b)$$

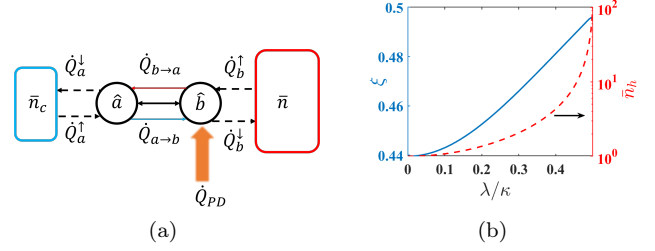


FIG. 1. (a) Illustration for the heat flux and heat transfer between the cavity(heat engine) and the mechanical oscillator(quantum fuel) in the hot isochoric strokes. The mechanical parametric drive provides an external energy injection, while the optomechanical interaction transforms the energy from the "quantum fuel" to the heat engine. (b) Utilization efficiency and steady-state occupation numbers with parametric drive. Both the ξ and the \bar{n}_h are calculated under resonant case $\Delta = \omega_M$. Other parameters are chosen as $G = \kappa$, $\gamma = 10^{-2}\kappa$, $\bar{n}_c = 0.01$ and $\bar{n} = 100$.

The detailed derivation is given in Appendix A, here \dot{Q}_x indicates the different contribution for the heat flux. As illustrated in Fig. 1(a), \dot{Q}_{PD} is the energy injection via mechanical parametric drive, $\dot{Q}_{b \rightarrow a}$ indicates heat flux transferred from the fuel to the heat engine, \dot{Q}_i^\uparrow ($i = a, b$) is the heating flux from the reservoir, \dot{Q}_i^\downarrow ($i = a, b$) is the dissipating flux. The exact form of these heat flux terms can be derived from the master equation(Eq. (2)),

$$\dot{Q}_{b \rightarrow a} = i\omega_M G(\langle a^\dagger b \rangle - \langle ab^\dagger \rangle), \quad (5a)$$

$$\dot{Q}_{\text{PD}} = \omega_M \lambda(\langle b^{\dagger 2} \rangle + \langle b^2 \rangle), \quad (5b)$$

$$\dot{Q}_b^\uparrow = \omega_M \gamma \bar{n}(\langle b^\dagger b \rangle + 1), \quad (5c)$$

$$\dot{Q}_b^\downarrow = -\omega_M \gamma(\bar{n} + 1)\langle b^\dagger b \rangle. \quad (5d)$$

The definition of utilization efficiency of energy for the mechanical mode is

$$\xi = \frac{-\dot{Q}_{b \rightarrow a}}{\dot{Q}_{\text{PD}} + \dot{Q}_b^\uparrow}, \quad (6)$$

and the steady state occupation of photon mode is defined as $\bar{n}_h = \langle a^\dagger a \rangle_{ss}$. The steady-state utilization efficiency of energy produced from the quantum fuel, and the effective thermal occupations for the cavity, are plotted in Fig. 1(b). Compared with the standard optomechanical interaction case ($\lambda = 0$), the external mechanical driven term generates additional energy injection, which supplies more energy than just extracted from the mechanical thermal bath. From the view of quantum thermodynamics, the larger steady-state occupation for the cavity indicates higher inner energy differences, which reflects more heat absorption or work production. On the other hand, following the discussion of heat flux for the total system, the larger parametric drive strength leads to the higher utilization efficiency of energy, thus more heat is transmitted from the mechanical mode into the

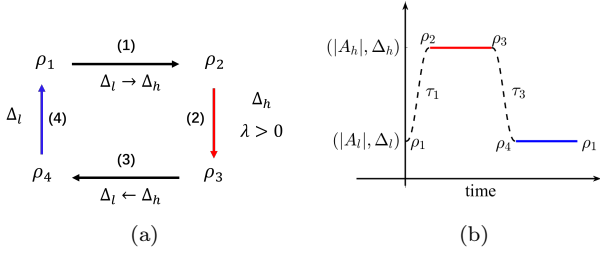


FIG. 2. (a) The quantum Otto cycle for the cavity by tuning the detuning to produce the extra work output, and turning the parametric drive on and off to "heating" and "cooling" the cavity. (b) Amplitude and detuning for the laser drive in an Otto-type cycle.

cavity. Therefore, the cavity has a stronger ability to extract heat from the additional effective heat bath. Both of the above qualities indicate that in this optomechanical model, the cavity is a suitable candidate for heat engines used to produce mechanical output work, while the mechanical mode, which injects the additional heat into the engine and creates an effective hot thermal reservoir, has been acting as the quantum fuel.

B. Quantum Otto-type Cycle

A typical Otto cycle is constructed by two isentropic and two adiabatic processes. In the isentropic process, the engine is in contact with the hot(cold) thermal bath and has the energy exchange, while in the adiabatic process, the engine does not have thermal contact with the environment and just produces work. However, in quantum scenarios, the adiabatic processes not only satisfy the thermal adiabaticity that the system has zero thermal exchange but also follow the quantum adiabatic dynamics [6, 10, 34]. Thus, we call the former case quantum Otto-type cycle.

By changing the mechanical parametric drive strength λ in different steps, the quantum Otto-type cycle in our model, illustrated in Fig. 2, can be constructed as follows:

(1). Isentropic compression($\rho_1 \rightarrow \rho_2$), the cavity detuning $\Delta(t)$ and the amplitude of laser drive A will be changed from (Δ_l, A_l) to (Δ_h, A_h) simultaneously during time τ to fix the classical part of the cavity mode. During this stroke, $\lambda = 0$.

(2). Hot isochoric($\rho_2 \rightarrow \rho_3$), the optomechanical sys-

tem with mechanical parametric drive λ , the cavity detuning $\Delta = \Delta_h = \omega_M$ is fixed. Then the system under the frame rotating ω_M is

$$H_h = G(ab^\dagger + a^\dagger b) + \frac{i}{2}\lambda(b^{\dagger 2} - b^2), \quad (7)$$

the steady-state occupation for the cavity mode after this stroke is \bar{n}_h . The system under the hot isochoric stroke has the stability condition that $\lambda \leq \min\{\frac{\gamma}{2}(1+C_0), \frac{\gamma+\kappa}{2}\}$, where $C_0 = 4G^2/\kappa\gamma$.

(3). Isentropic expansion($\rho_3 \rightarrow \rho_4$), during this stroke the cavity detuning will reverse to Δ_l via $\Delta(\tau - t)$, the heat engine will produce positive work.

(4). Cold isochoric($\rho_4 \rightarrow \rho_1$), the system evolves to the steady state without mechanical parametric drive ($\lambda = 0$), the cavity detuning is fixed at Δ_l .

To design the two isentropic strokes, the evolution time $\tau \ll 1/\kappa$ is achieved to neglect the energy dissipation. In the weak interacting $G \ll \omega_M$ and resolved sideband $\kappa \ll \omega_M$ regimes, the optomechanical interaction would only be resonantly enhanced. Hence, in the large detuned case, $|\Delta_l - \Delta_h| \gg \kappa$, the steady state for cavity in the cold isochoric stroke would almost be the thermal state with average occupation \bar{n}_c , and the optomechanical interaction term can be regarded as perturbations in analyzing the two isentropic strokes.

We first neglect the optomechanical interaction in the two isentropic strokes. The work production and heat absorption in a quantum Otto cycle can be defined with the two-point measurement approach, in which the energy change for the heat engine is obtained by projective measurement at the beginning and the end of each strokes [32]. The joint probability distribution for an Otto cycle has the form [20]

$$P(W, Q) = \sum_{m,n,j,k} \delta [W - (E_j^l - E_k^h + E_m^h - E_n^l)] \times \delta [Q - (E_k^h - E_m^h)] P_{n \rightarrow m}^\tau P_{k \rightarrow j}^\tau P_n(\bar{n}_c) P_j(\bar{n}_h). \quad (8)$$

Here $P_{n \rightarrow m}^\tau$ and $P_{k \rightarrow j}^\tau$ indicate the transition probabilities from initial eigenstates $n(k)$ to the final eigenstates $m(j)$ for the isentropic strokes, and $P_n(N) = (1/(1+N))(N/(1+N))^n$ is the probability distribution for the thermal states with occupation N .

For the calculation of average net work output and heat absorbed per cycle, the characteristic function of the joint probability distribution is

$$\chi(u, v) = \int dW dQ e^{iuW} e^{ivQ} P(W, Q) = \chi_h(u, v) \chi_l(u, v), \quad (9)$$

$$\chi_l(u, v) = \frac{\sqrt{2}}{\bar{n}_c + 1} \{ Q^* (1 - e^{i2(u-v)\Delta_h}) [1 - e^{-i2u\Delta_l} (\frac{\bar{n}_c}{\bar{n}_c + 1})^2] + (1 + e^{i2(u-v)\Delta_h}) [1 + e^{-i2u\Delta_l} (\frac{\bar{n}_c}{\bar{n}_c + 1})^2] - 4e^{i(u-v)\Delta_h} e^{-iu\Delta_l} (\frac{\bar{n}_c}{\bar{n}_c + 1}) \}^{-1/2}, \quad (10)$$

$$\chi_h(u, v) = \frac{\sqrt{2}}{\bar{n}_h + 1} \left\{ Q^* (1 - e^{i2u\Delta_l}) [1 - e^{-i2(u-v)\Delta_h} \left(\frac{\bar{n}_h}{\bar{n}_h + 1}\right)^2] + (1 + e^{i2u\Delta_l}) [1 + e^{-i2(u-v)\Delta_h} \left(\frac{\bar{n}_h}{\bar{n}_h + 1}\right)^2] - 4e^{-i(u-v)\Delta_h} e^{iu\Delta_l} \left(\frac{\bar{n}_h}{\bar{n}_h + 1}\right) \right\}^{-1/2}. \quad (11)$$

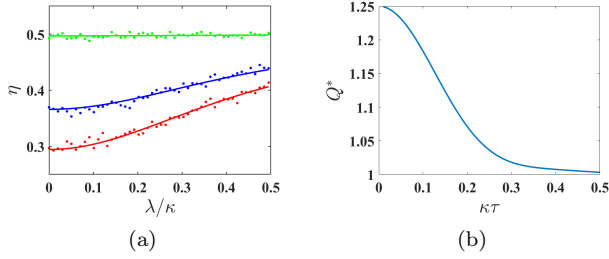


FIG. 3. (a) The non-adiabatic thermal efficiencies (Eq. (13)). The red, blue, and green lines correspond to the chosen evolution time $\tau = 0.1/\kappa$, $0.15/\kappa$ and $0.5/\kappa$, respectively. The solid lines are the analytical results, while the dots are the numerical simulation results. (b) The adiabatic parameter under different τ . In both plots, Q^* is calculated with the detuning as Eq. (16), other parameters are chosen as $\Delta_h = 20\kappa$, $\Delta_l = \Delta_h/2$, $\omega_M = \Delta_h$, $\bar{n} = 100$, $\bar{n}_c = 0.01$ and $\gamma = 0.01\kappa$.

The average work and heat absorbed from the effective hot reservoir are obtained from the characteristic function [21]

$$\langle W \rangle_{Q^*} = -i \frac{\partial \ln \chi(u, v)}{\partial u} \Big|_{u=v=0}, \quad (12a)$$

$$\langle Q \rangle_{Q^*} = -i \frac{\partial \ln \chi(u, v)}{\partial v} \Big|_{u=v=0}. \quad (12b)$$

The thermal efficiency can be derived as

$$\eta_{\text{th}} = 1 - \frac{\Delta_l Q^* (\bar{n}_h + 1/2) - (\bar{n}_c + 1/2)}{\Delta_h (\bar{n}_h + 1/2) - Q^* (\bar{n}_c + 1/2)}. \quad (13)$$

Here Q^* is the adiabatic parameter, for $Q^* = 1$ is the quantum adiabatic condition while $Q^* > 1$ the non-adiabatic scattering occurs [1]. Fig. 3 indicates that the dissipation can be safely neglected when the evolution time in the two isentropic processes is small.

III. WORK GENERATION AND EFFICIENCIES

So far the heat absorption in a quantum Otto-type cycle is discussed. To describe quantum heat engines, work generation is another important process to determine thermal efficiency. Below we will discuss the two strokes in the quantum Otto-type cycle that generate work.

The quantum Otto engine reaches its maximal thermal efficiency when the isentropic strokes evolve quantum adiabaticity ($Q^* = 1$), with which the adiabatic Otto

efficiency $\eta_{\text{Qtto}} = 1 - \Delta_l/\Delta_h$. However, the quantum adiabatic condition requires the dynamical evolution of the system to be slow enough that the non-adiabatic transitions between different eigenstates can be neglected, and the system follows the instantaneous eigenstates in time. Therefore, even if the quantum adiabatic processes would have maximal efficiency, the power for the total work generation is zero. To obtain the efficiency close to the adiabatic case in finite time, the shortcut-to-adiabaticity (STA) technique [5, 23] has been considered.

Here we use the counter-diabatic driving (CD) method to realize STA. The basic method is to find a driving Hamiltonian, with which the exact solution for the total Hamiltonian including the driving term, is the adiabatic approximating result for the original Hamiltonian [30]. The CD Hamiltonian has the form [5]

$$H_{\text{STA}}(t) = i \frac{\dot{\Delta}_t}{4\Delta_t} (a^2 - a^{\dagger 2}). \quad (14)$$

The STA method has boundary conditions, which ensures the CD term vanishes at the initial and the final time,

$$\begin{aligned} \Delta_i &= \Delta_{l(h)}, \quad \Delta_f = \Delta_{h(l)}, \\ \dot{\Delta}_{t=0} &= \dot{\Delta}_{t=\tau} = 0, \\ \ddot{\Delta}_{t=0} &= \ddot{\Delta}_{t=\tau} = 0. \end{aligned} \quad (15)$$

As an example, we can choose the detuning in compression strokes [5]

$$\begin{aligned} \Delta_t &= \Delta_i + 10(\Delta_f - \Delta_i)(t/\tau)^3 \\ &\quad - 15(\Delta_f - \Delta_i)(t/\tau)^4 + 6(\Delta_f - \Delta_i)(t/\tau)^5, \end{aligned} \quad (16)$$

where $\Delta_i = \Delta_l$, $\Delta_f = \Delta_h$. The expansion strokes have the detuning $\Delta_{(\tau-t)}$ with opposite initial and final values compared with compression strokes.

As we have analyzed in Sec. II, the optomechanical interaction induces an effective hot thermal bath for the heat engine. Thus, the additional CD term changes the thermal occupation for the cavity, which indicates additional heat absorption during compression/expansion strokes. The average value for the corresponding process is $\langle H_{\text{STA}}^{c/e} \rangle_\tau = \frac{1}{\tau} \int_0^\tau dt \langle H_{\text{STA}}^{c/e}(t) \rangle$, where the instantaneous expectation value can be obtained

$$\langle H_{\text{STA}}^{c/e}(t) \rangle = \frac{\Delta_{t/(\tau-t)}}{\Delta_i} \langle H(0) \rangle \left(\frac{\Delta_{t/(\tau-t)}}{\Omega_{t/(\tau-t)}} - 1 \right), \quad (17)$$

here the superscript c/e indicates the compression/expansion processes, and $\Omega_{t/(\tau-t)} =$

$\Delta_{t/(\tau-t)}\sqrt{1 - \dot{\Delta}_{t/(\tau-t)}^2/4\Delta_{t/(\tau-t)}^4}$ [31] is the modified eigen-frequency for the total system that includes the CD term. Thus in the STA evolution, the parameters should be chosen to keep $\Omega_{t/(\tau-t)} > 0$, and the modified efficiency has the form

$$\eta_{STA} = -\frac{\langle W \rangle_{Q^*=1}}{\langle Q \rangle_{Q^*=1} + \sum_{j=c,e} \langle H_{STA}^j \rangle_{\tau}}. \quad (18)$$

A. Extra heat produced by optomechanical interaction

So far we have discussed the quantum Otto heat engine whose cavity acts as the working fluid in an optomechanical system with mechanical parametric drive by neglecting the optomechanical interacting term in the two isentropic strokes. Hence, in the compression/expansion processes, the optomechanical system is equivalent to two independent harmonic oscillators, the time-dependent cavity detuning only produces work. However, the optomechanical interaction can not be turned on and off straightforwardly, even weak coupling changes the energy for the cavity. Therefore, the external interaction leads to extra heat transfer between the cavity and the mechanical mode.

There are a few cases in which the OM interaction can be neglected in the work-producing processes, e.g., the detuning suddenly changes from initial to final values. In this case, the adiabatic parameter $Q^* = (\Delta_i^2 + \Delta_f^2)/2\Delta_i\Delta_f$ [1, 10] is larger than 1 and the STA process can not be realized. To realize STA, the time-dependent detuning (Eq.(16)) needs finite evolution time to satisfy the boundary condition (Eq. (15)), thus it leads to the extra heat transfer from the mechanical mode via the optomechanical interaction. In our quantum heat engine model, the mechanical mode acts as the quantum fuel, which provides an effective hot thermal reservoir to the cavity. Thus during the compression/expansion processes, the optomechanical interaction generates extra heat absorption.

The extra heat absorbed from the mechanical mode at time t can be written as

$$\begin{aligned} \Delta E^{c/e}(t) &= E_a^{\text{int},c/e}(t) - E_a^{0,c/e}(t), \\ E_a^{\text{int}/0,c/e}(t) &= \langle H_a(t) \rangle_{\text{int}/0} = \text{Tr}\{\rho^{\text{int}/0} H_a(t)\}. \end{aligned} \quad (19)$$

The superscript int/0 indicates within/without optomechanical interaction, and the $\rho^{\text{int}/0}$ corresponds to

$$\dot{\rho}^{\text{int}} = -i[H_a + H_b + H_{\text{int}}, \rho^{\text{int}}] + \mathcal{L}_{\text{diss}}\rho^{\text{int}}, \quad (20a)$$

$$\dot{\rho}^0 = -i[H_a + H_b, \rho^0] + \mathcal{L}_{\text{diss}}\rho^0, \quad (20b)$$

where the H_{int} indicates the optomechanical interaction term in Eq. (1). Similarly, the average heat absorption during compression/expansion processes is

$$\langle \Delta E^{c/e} \rangle_{\tau} = \frac{1}{\tau} \int_0^{\tau} dt \Delta E^{c/e}(t). \quad (21)$$

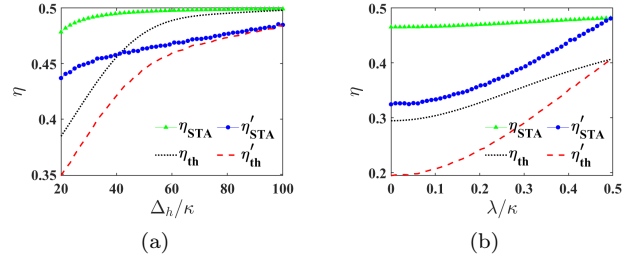


FIG. 4. Efficiencies for different controlling parameters under fixed τ . (a). Efficiencies for different detunings with a fixed ratio of $\Delta_l/\Delta_h = 1/2$, where the mechanical parametric driving strength $\lambda = 0.4\kappa$; (b). Efficiencies vs λ with the same ratio of $\Delta_l/\Delta_h = 1/2$ and fixed $\Delta_h = 20\kappa$. In both plots, the evolution time has been chosen as $\kappa\tau = 0.1$. Other parameters for both plots are chosen as $\bar{n}_c = 0.01$, $\bar{n} = 100$, $G = \kappa$, $\gamma = 0.01\kappa$ and $\omega_M = \Delta_h$.

Thus the modified efficiency is

$$\eta'_{STA} = -\frac{\langle W \rangle_{Q^*=1}}{\langle Q \rangle_{Q^*=1} + \sum_{j=c,e} \langle H_{STA}^j \rangle_{\tau} + \langle \Delta E^j \rangle_{\tau}}. \quad (22)$$

The thermal efficiency within the optomechanical interaction η'_{th} can be easily obtained by the above procedure. The efficiencies for the fixed evolution time τ are plotted in Fig. 4. In both plots, the nonadiabatic efficiencies are calculated by Eq. (13), the modification for the heat absorption induced by the optomechanical interaction is added to the total heat absorption, and the detuning was tuned following the Eq. (16). The efficiencies for the STA methods that neglect and include the extra heat terms are calculated by Eq.(18) and Eq. (22), respectively. It has been noted that as Δ_h and Δ_l increase, the STA Hamiltonian(Eq. (14)) has less contribution to the system evolution, the system evolves near the instantaneous eigenstates once the boundary conditions are fulfilled. Meanwhile, because the contribution to the total heat absorption in a thermodynamic cycle has three parts, heat absorbing from the effective hot thermal reservoir $\langle Q \rangle$, the counter-diabatic driving $\langle H_{STA}^{c/e} \rangle_{\tau}$ and the extra heat from the optomechanical interaction(Eq. (21)), the contribution for the latter two terms is mainly determined by the evolution time for the two strokes, thus the influence of these two parts decreases as mechanical parametric driving strength increases.

B. Optimal Efficiency Control

Compared with the traditional thermodynamical cycle, a finite-time heat engine explicitly accounts for finite-time cycles, which generate non-zero power output. To obtain the higher output power, the evolution time in working processes is required as short as possible. In our model, due to the limit condition $\Omega_t > 0$ to avoid

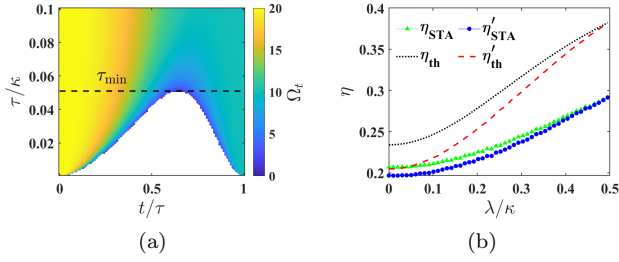


FIG. 5. (a) The minimal τ in the compression process, which is obtained for $\Omega_t > 0$, the white area in the plot means trap inversion occurs. (b) Efficiency at minimal τ vs λ . The corresponding τ_{\min} is obtained numerically. Other parameters are chosen the same as Fig. 4.

the trap inversion [5], there exists the shortest evolution time in compression/expansion strokes. Below this limit, Ω_t becomes a complex value, the STA path breaks down.

Fig. 5(a) illustrates the minimal evolution time τ_{\min} in the working strokes. The corresponding efficiencies for the heat engine under the τ_{\min} are plotted in Fig. 5(b), with the same corresponding efficiencies as in Fig. 4. It has been noticed that under the τ_{\min} in the two working strokes, $\eta_{\text{STA}} < \eta_{\text{th}}$. For a time-dependent system, the faster time evolution usually has a larger non-adiabatic scattering rate, thus, the CD term needs higher extra energy to limit the system evolution close to the adiabatic eigenstates, the heat exchange induced by the STA path $\langle H_{\text{STA}}^{c/e} \rangle_{\tau}$, has a significant influence on the thermal efficiencies. Therefore, although the working processes have the largest output power, the STA path in τ_{\min} leads to an efficiency even smaller than the non-adiabatic thermal efficiency.

Because the STA process leads to additional heat absorption in working strokes $\langle H_{\text{STA}}^{c/e} \rangle_{\tau}$ is τ -dependent. Therefore, a critical evolution time exists to distinguish whether the STA efficiency (Eq. (18)) is larger than the non-adiabatic thermal efficiency (Eq. (13)) or not. Under the critical evolution time τ_{cri} , $\eta_{\text{th}} = \eta_{\text{STA}}$, which suggests

$$\sum_{j=c,e} \langle H_{\text{STA}}^j \rangle_{\tau} = \frac{\langle W \rangle_{Q^*=1} \langle Q \rangle}{\langle W \rangle} - \langle Q \rangle_{Q^*=1}. \quad (23)$$

The minimal τ , which is obtained for the Ω_t , is independent of the parametric drive strength λ . The critical time τ_{cri} is defined to hold the critical condition (Eq. (23)) that the contribution of heat absorption of the STA counteracts the non-adiabatic effect, which becomes larger when λ increase, as plotted in Fig. 6(a). However, the optomechanical interaction has not been considered in the discussion for the τ_{cri} above. To consider the heat exchange $\langle \Delta E^{c/e} \rangle_{\tau}$ induced by the optomechanical interaction, because of $\bar{n} \gg \bar{n}_c$, in our system, the interaction leads to the extra heat absorption to the engine, with which $\sum_{j=c,e} \langle \Delta E^j \rangle_{\tau} > 0$. Therefore, under the critical

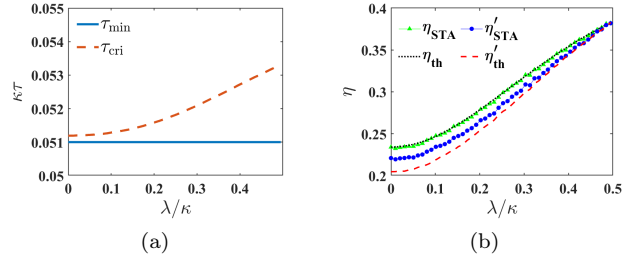


FIG. 6. (a). Minimal and critical evolution time. (b). Efficiencies at the critical time τ_{cri} . The black dotted line is η_{th} ; the green triangle is η_{STA} ; the purple dashed line is the thermal efficiency within the optomechanical interaction, η'_{th} ; the blue circle is η'_{STA} . Other parameters for both plots are the same as Fig. 4.

condition that ignored the optomechanical interaction, $\eta'_{\text{STA}} > \eta'_{\text{th}}$, as Fig. 6(b) suggested. It also suggests the optomechanical interaction decreases the τ_{cri} .

IV. CONCLUSIONS AND DISCUSSIONS

We proposed a quantum heat engine model in a standard optomechanical system with an additional mechanical parametric drive term. We find the non-equilibrium steady-state exhibits an amplification for cavity excitation, which is equivalent to an effective thermal distribution with high thermal occupations for the photon mode. A cyclic quantum Otto-type heat engine that the cavity as working fluid is discussed, and the engine in contact with effective hot and cold thermal baths can be realized by switching the mechanical parametric drive on and off. We also discussed heat extraction from the auxiliary quantum system, which can be designed as quantum fuel. The utilization efficiency for the quantum fuel is defined. In our model, the thermal efficiency and the utilization efficiency of energy have been enhanced simultaneously via the additional parametric mechanical drive. Our study might be useful for later research on energy transformation and supplements in quantum devices.

ACKNOWLEDGMENTS

Y.D.W. acknowledges support from the Fundamental and Interdisciplinary Frontier Research Priority Program of Chines Academy of Sciences (Grant No. XDB0920102), NSFC (Grant No.12275331) and the Penghuanwu Innovative Research Center (Grant No. 12047503).

Appendix A: Heat flux

The equations for the heat flux (Eq. (4, 5)) in the main text can be derived from the master equation (Eq. (2)). Using the equation $\partial_t \langle O \rangle = \text{Tr}\{\dot{\rho}O\}$, we have

$$\begin{aligned} \frac{d\langle H_a \rangle}{dt} &= -i\text{Tr}\{[H_{\text{int}}, \rho]H_a\} \\ &\quad + \kappa(\bar{n}_c + 1)\text{Tr}\{D[a]\rho H_a\} + \kappa\bar{n}_c\text{Tr}\{D[a^\dagger]\rho H_a\}, \end{aligned} \quad (\text{A1})$$

$$\begin{aligned} \frac{d\langle H_b \rangle}{dt} &= -i\text{Tr}\{[H_{\text{int}}, \rho]H_b\} - i\text{Tr}\{[H_{\text{PD}}, \rho]H_b\} \\ &\quad + \gamma(\bar{n} + 1)\text{Tr}\{D[b]\rho H_b\} + \gamma\bar{n}\text{Tr}\{D[b^\dagger]\rho H_b\}. \end{aligned} \quad (\text{A2})$$

Here the H_{int} and H_{PD} correspond to the interaction and mechanical parametric drive terms, respectively. Each part of the above equations indicates the energy transformation between two subsystems H_a and H_b , as illustrated in Fig. 1(a). If we define

$$\dot{Q}_{a(b) \rightarrow b(a)} = -i\text{Tr}\{[H_{\text{int}}, \rho]H_{b(a)}\}, \quad (\text{A3a})$$

$$\dot{Q}_{\text{PD}} = -i\text{Tr}\{[H_{\text{PD}}, \rho]H_b\}, \quad (\text{A3b})$$

$$\dot{Q}_a^\dagger = \kappa\bar{n}_c\text{Tr}\{D[a^\dagger]\rho H_a\}, \quad (\text{A3c})$$

$$\dot{Q}_a^\downarrow = \kappa(\bar{n}_c + 1)\text{Tr}\{D[a]\rho H_a\}, \quad (\text{A3d})$$

$$\dot{Q}_b^\dagger = \gamma\bar{n}\text{Tr}\{D[b^\dagger]\rho H_b\}, \quad (\text{A3e})$$

$$\dot{Q}_b^\downarrow = \gamma(\bar{n} + 1)\text{Tr}\{D[b]\rho H_b\}, \quad (\text{A3f})$$

then the exact form of Eq. (4,5) can be obtained.

Appendix B: The Fokker-Planck Equation

The master equation (Eq. (2)) with the hot isochoric Hamiltonian (Eq.(7)) can be easily transformed into the phase space, with the positive-P function Fokker-Planck equation form

$$\frac{\partial P(\vec{\alpha}, t)}{\partial t} = \left(-\vec{\alpha}'^T A \vec{\alpha} + \frac{1}{2} \vec{\alpha}'^T D \vec{\alpha}' \right) P(\vec{\alpha}, t), \quad (\text{B1})$$

where $\vec{\alpha} = (\alpha, \alpha^*, \beta, \beta^*)^T$, $\vec{\alpha}' = (\partial/\partial\alpha, \partial/\partial\alpha^*, \partial/\partial\beta, \partial/\partial\beta^*)^T$,

$$A = \begin{pmatrix} -\kappa/2 & 0 & -iG & 0 \\ 0 & -\kappa/2 & 0 & iG \\ -iG & 0 & -\gamma/2 & \lambda \\ 0 & iG & \lambda & -\gamma/2 \end{pmatrix} \quad (\text{B2})$$

$$D = \begin{pmatrix} 0 & \kappa\bar{n}_c & 0 & 0 \\ \kappa\bar{n}_c & 0 & 0 & 0 \\ 0 & 0 & \lambda & \gamma\bar{n} \\ 0 & 0 & \gamma\bar{n} & \lambda \end{pmatrix}. \quad (\text{B3})$$

The matrix A can be diagonalized as $\tilde{A} = SAS^{-1} = \text{diag}(k_1, k_2, k_3, k_4)$, where

$$\begin{aligned} k_{1(2)} &= \frac{1}{4} \sqrt{-\gamma - \kappa - 2\lambda \mp \sqrt{(\gamma - \kappa + 2\lambda)^2 - 16G^2}} \\ k_{3(4)} &= \frac{1}{4} \sqrt{-\gamma - \kappa + 2\lambda \mp \sqrt{(\kappa - \gamma + 2\lambda)^2 - 16G^2}}. \end{aligned}$$

To let all the above four eigenvalues k_i have negative real parts, we can finally get the stability condition $\lambda \leq \min\{\gamma(1 + C_0)/2, (\gamma + \kappa)/2\}$.

Following the Green's function method, we obtained the steady state solution of Eq. (B1)

$$P_{ss}(\vec{\alpha}) = \frac{1}{\sqrt{(2\pi)^4 \det |Q_{ss}|}} \exp\left(-\frac{1}{2} \vec{\alpha}^T Q_{ss}^{-1} \vec{\alpha}\right), \quad (\text{B4})$$

with $Q_{ss} = S^{-1} \tilde{Q}_{ss} (S^{-1})^T$, $(\tilde{Q}_{ss})_{ij} = -\tilde{D}_{ij}/(k_i + k_j)$ and $\tilde{D} = SDS^T$. Then the steady-state correlations can be solved

$$\langle O_i O_j \rangle_{ss} = (Q_{ss})_{ij}, \quad (\text{B5})$$

where $\vec{O} = (a, a^\dagger, b, b^\dagger)^T$. Therefore, the steady-state photon occupation and correlations which reflected the utilization efficiency of energy have the form

$$\begin{aligned} \langle a^\dagger a \rangle_{ss} &= \frac{1}{2} \left\{ \frac{\kappa\bar{n}_c(\gamma - 2\lambda)(\gamma + \kappa - 2\lambda) + 4G^2(\gamma\bar{n} + \kappa\bar{n}_c + \lambda)}{[4G^2 + \kappa(\gamma - 2\lambda)](\gamma + \kappa - 2\lambda)} \right. \\ &\quad \left. + \frac{\kappa\bar{n}_c(\gamma + 2\lambda)(\gamma + \kappa + 2\lambda) + 4G^2(\gamma\bar{n} + \kappa\bar{n}_c - \lambda)}{[4G^2 + \kappa(\gamma + 2\lambda)](\gamma + \kappa + 2\lambda)} \right\}, \end{aligned} \quad (\text{B6})$$

$$\begin{aligned} \langle b^\dagger b \rangle_{ss} &= \frac{1}{2} \left\{ \frac{\kappa(\gamma + \kappa - 2\lambda)(\bar{n}\gamma + \lambda) + 4G^2(\gamma\bar{n} + \kappa\bar{n}_c + \lambda)}{[4G^2 + \kappa(\gamma - 2\lambda)](\gamma + \kappa - 2\lambda)} \right. \\ &\quad \left. + \frac{\kappa(\gamma + \kappa + 2\lambda)(\bar{n}\gamma - \lambda) + 4G^2(\gamma\bar{n} + \kappa\bar{n}_c - \lambda)}{[4G^2 + \kappa(\gamma + 2\lambda)](\gamma + \kappa + 2\lambda)} \right\}, \end{aligned} \quad (\text{B7})$$

$$\begin{aligned} \langle a^\dagger b \rangle_{ss} &= iG\kappa \left\{ \frac{(\bar{n} - \bar{n}_c)\gamma + (1 + 2\bar{n}_c)\lambda}{[4G^2 + \kappa(\gamma - 2\lambda)](\gamma + \kappa - 2\lambda)} \right. \\ &\quad \left. + \frac{(\bar{n} - \bar{n}_c)\gamma - (1 + 2\bar{n}_c)\lambda}{[4G^2 + \kappa(\gamma + 2\lambda)](\gamma + \kappa + 2\lambda)} \right\}, \end{aligned} \quad (\text{B8})$$

$$\begin{aligned} \langle b^2 \rangle_{ss} &= \left\{ \frac{\kappa(\gamma + \kappa - 2\lambda)(\bar{n}\gamma + \lambda) + 4G^2(\gamma\bar{n} + \kappa\bar{n}_c + \lambda)}{[4G^2 + \kappa(\gamma - 2\lambda)](\gamma + \kappa - 2\lambda)} \right. \\ &\quad \left. - \frac{\kappa(\gamma + \kappa + 2\lambda)(\bar{n}\gamma - \lambda) + 4G^2(\gamma\bar{n} + \kappa\bar{n}_c - \lambda)}{[4G^2 + \kappa(\gamma + 2\lambda)](\gamma + \kappa + 2\lambda)} \right\}. \end{aligned} \quad (\text{B9})$$

Appendix C: stochastic differential equations

The above Fokker-Planck equation (Eq. B1) in different scenarios is equivalent to the Ito stochastic differential equation, which has the form

$$d\vec{\alpha}_t^{\text{int}/0,c/e} = A(\vec{\alpha}_t^{\text{int}/0,c/e})dt + B(\vec{\alpha}_t^{\text{int}/0,c/e})d\vec{W}_t, \quad (\text{C1})$$

where $\vec{\alpha}_t$ is the column vector formed from the families of random variables $\vec{\alpha}_{1t}, \dots, \vec{\alpha}_{nt}$, each n indicates a group of independent trajectories in phase space; $A(\vec{\alpha}_t^{\text{int}/0,c/e})$ is the drift term, while the matrix $B(\alpha_t^{\text{int}/0,c/e})$ is defined

by the diffusion matrix:

$$D(\alpha) = B(\alpha)B(\alpha)^T. \quad (\text{C2})$$

And \vec{W}_t indicates n independent Wiener process, which in the short time limit is the term of Gaussian white noise. The matrix $A^{\text{int}/0,c/e}, B^{c/e}$ have the form

$$A^{\text{int},c/e} = \begin{pmatrix} -\kappa/2 - i\Delta_t/(\tau-t) & 0 & -iG & 0 \\ 0 & -\kappa/2 + i\Delta_t/(\tau-t) & 0 & iG \\ -iG & 0 & -\gamma/2 - i\omega_M & 0 \\ 0 & iG & 0 & -\gamma/2 + i\omega_M \end{pmatrix}, \quad (\text{C3})$$

$$A^{0,c/e} = \begin{pmatrix} -\kappa/2 - i\Delta_t/(\tau-t) & 0 & 0 & 0 \\ 0 & -\kappa/2 + i\Delta_t/(\tau-t) & 0 & 0 \\ 0 & 0 & -\gamma/2 - i\omega_M & 0 \\ 0 & 0 & 0 & -\gamma/2 + i\omega_M \end{pmatrix}, \quad (\text{C4})$$

$$B^{c/e} = \frac{1}{\sqrt{2}} \begin{pmatrix} i\sqrt{\kappa\bar{n}_h/c} & \sqrt{\kappa\bar{n}_h/c} & 0 & 0 \\ -i\sqrt{\kappa\bar{n}_h/c} & \sqrt{\kappa\bar{n}_h/c} & 0 & 0 \\ 0 & 0 & i\sqrt{\gamma\bar{n}} & \sqrt{\gamma\bar{n}} \\ 0 & 0 & -i\sqrt{\gamma\bar{n}} & \sqrt{\gamma\bar{n}} \end{pmatrix} \quad (\text{C5})$$

Thus the instantaneous inner energy for the cavity can be calculated as

$$E_{\text{cav}}^{\text{int}/0,c/e}(t) = \Delta_t/(\tau-t) (\langle \alpha_1^{\text{int}/0} \alpha_2^{\text{int}/0} \rangle + 1/2). \quad (\text{C6})$$

-
- [1] K. Husimi, *Progress of Theoretical Physics* **9**, 381 (1953).
[2] R. Kosloff and A. Levy, *Annu Rev Phys Chem* **65**, 365 (2014).
[3] B. A. Levitan, A. Metelmann, and A. A. Clerk, *New Journal of Physics* **18**, 093014 (2016).
[4] D. Bothner, S. Yanai, A. Iniguez-Rabago, M. Yuan, Y. M. Blanter, and G. A. Steele, *Nature Communications* **11**, 1589 (2020).
[5] O. Abah and E. Lutz, *Phys. Rev. E* **98**, 032121 (2018).
[6] H. T. Quan, Y.-x. Liu, C. P. Sun, and F. Nori, *Phys. Rev. E* **76**, 031105 (2007).
[7] S. Deffner and E. Lutz, *Phys. Rev. E* **77**, 021128 (2008).
[8] S. Deffner, O. Abah, and E. Lutz, *Chemical Physics* **375**, 200 (2010).
[9] S. Vinjanampathy and J. Anders, *Contemporary Physics* **57**, 545 (2016).
[10] O. Abah, J. Rossnagel, G. Jacob, S. Deffner, F. Schmidt-Kaler, K. Singer, and E. Lutz, *Phys Rev Lett* **109**, 203006 (2012).
[11] J. Rossnagel, O. Abah, F. Schmidt-Kaler, K. Singer, and E. Lutz, *Phys Rev Lett* **112**, 030602 (2014).
[12] R. Wulfert, M. Oechsle, T. Speck, and U. Seifert, *Phys Rev E* **95**, 050103 (2017).
[13] A. Levy and R. Kosloff, *EPL (Europhysics Letters)* **107**, 20004 (2014).
[14] G. De Chiara, G. Landi, A. Hewgill, B. Reid, A. Ferraro, A. J. Roncaglia, and M. Antezza, *New Journal of Physics* **20**, 113024 (2018).
[15] R. J. de Assis, T. M. de Mendonca, C. J. Villas-Boas, A. M. de Souza, R. S. Sarthour, I. S. Oliveira, and N. G. de Almeida, *Phys Rev Lett* **122**, 240602 (2019).
[16] G. Verley, M. Esposito, T. Willaert, and C. Van den Broeck, *Nat Commun* **5**, 4721 (2014).
[17] M. Campisi, J. Pekola, and R. Fazio, *New Journal of Physics* **17**, 035012 (2015).
[18] V. Holubec and A. Ryabov, *Journal of Physics A: Mathematical and Theoretical* **55**, 013001 (2021).
[19] T. Denzler and E. Lutz, *Phys. Rev. E* **98**, 052106 (2018).
[20] T. Denzler and E. Lutz, *Phys. Rev. Research* **2**, 032062 (2020).
[21] Z. Fei, J.-F. Chen, and Y.-H. Ma, *Phys. Rev. A* **105**, 022609 (2022).
[22] O. Abah and M. Paternostro, *Phys. Rev. E* **99**, 022110 (2019).
[23] D. Guéry-Odelin, A. Ruschhaupt, A. Kiely, E. Torrontegui, S. Martínez-Garaot, and J. G. Muga, *Rev. Mod. Phys.* **91**, 045001 (2019).
[24] J.-F. Chen, C.-P. Sun, and H. Dong, *Phys. Rev. E* **100**, 032144 (2019).
[25] J.-F. Chen, C.-P. Sun, and H. Dong, *Phys. Rev. E* **100**, 062140 (2019).
[26] A. Dechant, N. Kiesel, and E. Lutz, *Phys. Rev. Lett.* **114**, 183602 (2015).
[27] K. Zhang, F. Bariani, and P. Meystre, *Phys. Rev. Lett.* **112**, 150602 (2014).
[28] J. S. Bennett, L. S. Madsen, H. Rubinsztein-Dunlop, and

- W. P. Bowen, *New Journal of Physics* **22**, 103028 (2020).
- [29] J. Sheng, C. Yang, and H. Wu, *Science Advances* **7**, eabl7740 (2021).
- [30] M. P. Silveri, J. A. Tuorila, E. V. Thuneberg, and G. S. Paraoanu, *Reports on Progress in Physics* **80**, 056002 (2017).
- [31] H. Mishima and Y. Izumida, *Phys. Rev. E* **96**, 012133 (2017).
- [32] M. Esposito, U. Harbola, and S. Mukamel, *Rev. Mod. Phys.* **81**, 1665 (2009).
- [33] M. O. Scully, *Phys. Rev. Lett.* **88**, 050602 (2002).
- [34] J. Klatzow, J. N. Becker, P. M. Ledingham, C. Weinzetl, K. T. Kaczmarek, D. J. Saunders, J. Nunn, I. A. Walmsley, R. Uzdin, and E. Poem, *Phys. Rev. Lett.* **122**, 110601 (2019).
- [35] D. von Lindenfels, O. Gräß, C. T. Schmiegelow, V. Kaushal, J. Schulz, M. T. Mitchison, J. Goold, F. Schmidt-Kaler, and U. G. Poschinger, *Phys. Rev. Lett.* **123**, 080602 (2019).